Catalysis Science & Technology

PAPER

Cite this: *Catal. Sci. Technol.*, 2018, **8**, 2117

Highly-oriented one-dimensional MOF-semiconductor nanoarrays for efficient photodegradation of antibiotics†

Xiang He, [a] Vu Nguyen,[a] Zhang Jiang,[b] Dawei Wang, [a] Zan Zhu[a] and Wei-Ning Wang *[a]

Received 30th January 2018,
Accepted 11th March 2018

DOI: 10.1039/c8cy00229k

rsc.li/catalysis

The ineffective removal of antibiotics from the aquatic environment has raised serious problems, including chronic toxicity and antibiotic resistance. Among the numerous strategies, photocatalytic degradation appears to be one of the promising methods to remove antibiotics. Semiconductors are the most widely used photocatalysts, whereas, their efficiencies still suffer from limited light absorption and poor charge separation. Given their exceptional properties, including a superior surface area and massive active sites, MOFs are excellent candidates for the formation of hierarchical nanostructures with semiconductors to address the above issues. In this study, highly-oriented one-dimensional (1D) MIL-100(Fe)/TiO_2 nanoarrays were developed as photocatalysts for the first time (MIL = Materials Institute Lavoisier). The 1D structured TiO_2 nanoarrays not only enable the direct and enhanced charge transport, but also permit easy recycling. With the *in situ* growth of MIL-100(Fe) on the TiO_2 nanoarrays, the composite exhibits enhanced light absorption, electron/hole separation, and accessibility of active sites. As a result, up to 90.79% photodegradation efficiency of tetracycline, a representative antibiotic, by the MIL-100(Fe)/TiO_2 composite nanoarrays was achieved, which is much higher than that of pristine TiO_2 nanoarrays (35.22%). It is also worth mentioning that the composite nanoarrays demonstrate high stability and still exhibit high efficiency twice that of the pristine TiO_2 nanoarrays even in the 5th run. This study offers a new strategy for the degradation of antibiotics by using 1D MOF-based nanocomposite nanoarrays.

Introduction

Antibiotics have been extensively used for human, veterinary and agriculture purposes. However, due to the ineffectiveness of conventional wastewater treatment methods, massive amounts of antibiotics have been released into and accumulate in the aquatic environment, which can result in detrimental ecological consequences, including the occurrence and spread of antibiotic resistance and chronic toxicity to microbial species.[1,2] Thus, the development of efficient methods is in demand for the complete elimination of these antibiotics. Several approaches have been developed to remove antibiotics from water, including biological treatment, membrane separation, photocatalytic degradation and advanced oxidation processes (AOPs).[3] Among these, photocatalytic degradation appears to be one of the best choices because it is cost-effective and environmentally friendly.

Semiconductors, such as TiO_2, $BiVO_4$ and C_3N_4, are the most widely used photocatalysts for antibiotic degradation due to their outstanding photocatalytic ability and low cost.[4,5] However, semiconductor-based photocatalysts have two inherent drawbacks: limited light absorption and fast electron/hole recombination. The most widely used method to solve the aforementioned issues is to create semiconductor heterojunctions, with which not only the light absorption can be expanded but also the electron/hole separation can be efficiently promoted.[6] For instance, Hu *et al.*[7] constructed an all-solid-state Z-scheme photocatalytic system composed of Ag_2O, TiO_2 and reduced graphene oxide, where Ag_2O broadens the light absorption to a full spectrum and the Z-scheme system of rGO-Ag_2O/TiO_2 enables efficient charge transfer. This ternary composite was reported to exhibit promoted efficiency in the photodegradation of antibiotics even under near infrared light. Similarly, other heterojunctions, such as TiO_2/$Ni(OH)_2$,[8] $BiO_{1-x}Br/Bi_2O_2CO_3$ (ref. 9) and graphene-bridged Ag_3PO_4/Ag/$BiVO_4$,[10] also showed an enhanced photocatalytic ability towards the photodegradation of antibiotics. It should be noted that the surface area and porosity of the semiconductors are generally very small, which limits the amount and accessibility of the photoactive

[a] *Department of Mechanical and Nuclear Engineering, Virginia Commonwealth University, Richmond, Virginia 23219, USA. E-mail: wnwang@vcu.edu*
[b] *Advanced Photon Source, Argonne National Laboratory, Argonne, Illinois 60439, USA*

† Electronic supplementary information (ESI) available: Additional information of the film samples. See DOI: 10.1039/c8cy00229k

sites to the reactants, and thus the further improvement in photocatalytic efficiency. In this sense, it would be rational to create hierarchical nanostructures between semiconductors with porous materials.

Recently, metal–organic frameworks (MOFs) have gained much attention mainly due to their high surface area, high porosity, and tunable structures. MOFs are composed of metal clusters and organic linkers. The metal clusters can be viewed as semiconductor quantum entities, while the organic linkers are antennae, which can enhance the light absorption and then activate the metal clusters through linker-to-metal charge transfer (LMCT).[11] In addition, the high porosity of MOFs provides numerous reactive sites. Given all these unique properties of MOFs, efforts have been made to create semiconductor/MOF nanocomposites.[12–16] For example, In_2S_3@MIL-125(Ti) was synthesized by Wang *et al.*,[13] with which antibiotics can be efficiently photodegraded, which is attributed to the efficient charge transfer and synergistic effect between In_2S_3 and MIL-125(Ti). Similar synergy was also observed between C_3N_4 and ZIF-8, the composite of which can degrade 96% of the antibiotics after 1 hour of sunlight exposure as a result of efficient adsorption and rapid interfacial charge transfer.[12] Notably, most of the current semiconductor/MOF nanocomposites are limited to powder morphologies, where the recycling of the photocatalysts could be a potential problem. In terms of this, a thin film-structured composite would be more desirable.

Herein, a thin composite film composed of MIL-100(Fe) and highly-oriented TiO_2 nanoarrays was developed for the photo-degradation of antibiotics for the first time. The synthesis process is illustrated in Scheme 1. Specifically, aerosol vapor chemical deposition (ACVD) was applied to synthesize the TiO_2 nanoarrays.[17,18] In comparison with the powder structure, the structure of the nanoarrays permits easy recycling, which is also more favorable for photocatalysis owing to the direct pathway for photo-generated electrons and thus an increased electron transport rate.[18,19] As the next step, the TiO_2 nanoarrays were sequentially immersed in iron nitrate and trimesic acid (TMA) solutions for the *in situ* growth of MIL-100(Fe). In this highly-oriented one dimensional (1D) composite nanostructure, the TiO_2 nanoarrays and MIL are in intimate contact, ensuring the efficient charge transfer at the interface. The properties and photocatalytic abilities of the as-prepared nanoarrays were investigated in detail. Results show that, by taking advantage of the synergy between TiO_2 nanoarrays and MIL-100(Fe), the as-prepared 1D composite nanoarrays exhibited excellent photocatalytic performance towards the degradation of tetracycline, one of the most widely used antibiotics.[20] On the basis of the results, a plausible pathway for the photodegradation of tetracycline was proposed. The outcome of this work is expected to broaden the strategies for the efficient removal of antibiotics by using 1D MOF-based photocatalysts.

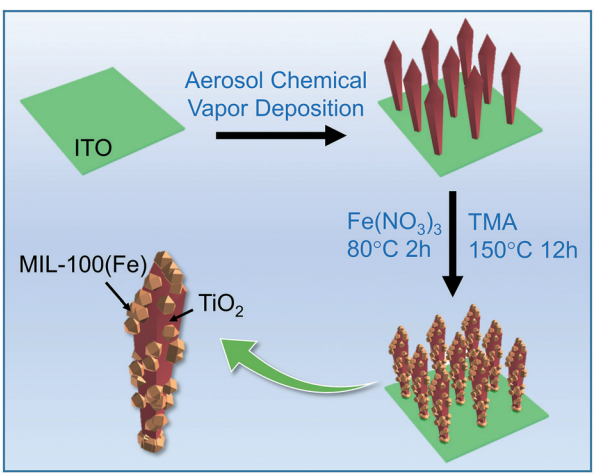

Scheme 1 Schematic illustration of the synthetic process of 1D TiO_2/MIL-100(Fe) composite nanoarrays (TMA: trimesic acid).

Experimental

Chemicals and synthesis

Titanium(IV) isopropoxide (TTIP, Alfa Aesar), iron(III) nitrate nonahydrate ($Fe(NO_3)_3{\cdot}9H_2O$, Sigma Aldrich) and trimesic acid (TMA, Sigma Aldrich) were used as received without further purification. The TiO_2 nanoarrays were synthesized on an ITO glass substrate (1.27 cm × 1.27 cm) by using TTIP as the precursor through the ACVD method.[18,21] To remove possible organic residues and increase the crystallinity of the TiO_2 nanoarrays, the as-prepared samples were calcined at 500 °C in air for 3 hours. Then, the TiO_2 nanoarrays were immersed into the $Fe(NO_3)_3{\cdot}9H_2O$ aqueous solution (0.8 to 20 mmol L^{-1}, 10 mL) at 80 °C for 2 hours. After that, the film was taken out and washed several times with deionized (DI) water to remove the residues. Subsequently, the film was put into an autoclave containing a saturated trimesic acid solution (0.3 g TMA in 4.28 mL DI water). The autoclave was then sealed and heated at 150 °C for 12 hours. After cooling down to room temperature, the MIL-100(Fe)/TiO_2 composite film was taken out and then immersed in ethanol to dissolve excess TMA, then flushed with DI water and dried in an air flow. The composite films are termed hereafter T/M-0.8 (to 20) (T = TiO_2, M = MIL-100(Fe)), where the numbers indicate the concentration (unit: mmol L^{-1}) of $Fe(NO_3)_3{\cdot}9H_2O$ used in the previous step.

Material characterization

The morphologies of the samples were analyzed by using a scanning electron microscope (SEM) equipped with energy-dispersive X-ray (EDX) spectroscopy (Su-70, Hitachi). X-ray diffraction (XRD) patterns were obtained with an X-ray diffractometer (PANalytical X'Pert Pro MPD). A UV-visible (UV-vis) spectrophotometer (Evolution 220, ThermoFisher) was used to investigate the optical properties of the samples. Vibrational spectral analysis was carried out with a Fourier transform infrared (FT-IR) spectrometer (Nicolet iS50, Thermo Scientific). X-ray photoelectron spectroscopy (XPS) measurements were conducted with a Thermo Scientific ESCALAB

250. Grazing-incidence wide-angle X-ray scattering (GIWAXS) measurements were carried out at the Advanced Photon Source (APS, beamline: 8-ID-E), Argonne National Laboratory. GIWAXS data were analyzed with the aid of the MATLAB toolbox, GIXSGUI.[22]

Photocatalysis analysis

Photodegradation of tetracycline was conducted in a quartz cuvette (inner dimension: 10 mm × 10 mm) at room temperature. In a typical photocatalysis experiment, a film sample was put into the quartz cuvette with a mixture of the tetracycline solution (100 mg L^{-1}, 3 mL) and hydrogen peroxide (30 wt%, 1 μL). The solution was stored in the dark for 30 min, then exposed to light irradiation provided by a Xe lamp (450 W, Newport). During the photodegradation process, the concentration of tetracycline was monitored every 10 min by using a UV-vis spectrophotometer.

Results and discussion

Material characterization

The SEM images of representative samples are shown in Fig. 1. The pristine TiO_2 films are composed of uniform nanoarrays (Fig. 1A and B) with a thickness of ~1.2 μm (Fig. S1†). The surfaces of pure TiO_2 nanoarrays are clean (Fig. 1B and S1†). After the growth of MIL-100(Fe), the composite retains the shape and dimensions (Fig. 1C). Meanwhile, the surfaces of the T/M composite become rough due to the presence of MIL-100(Fe) nanocrystals (Fig. 1D). Fig. 1E shows the EDX spectrum of the T/M composite (T/M-1.25), where the main elements (*i.e.*, Ti, Fe, C and O) are clearly identified. In addition, elemental mapping of the T/M composite (Fig. 1F) further reveals the uniform *in situ* growth of the MIL-100(Fe) crystals on the TiO_2 nanoarrays.

The crystal structures of the as-prepared samples were analyzed by XRD. As shown in Fig. 2A, several diffraction peaks were observed, stemming from ITO, TiO_2 and MIL-100(Fe). In particular, the TiO_2 nanoarrays have a main diffraction peak at 70.38° and a very small diffraction peak at 25.32°, corresponding to the (220) and (101) planes of anatase (JCPDS 21-1272), respectively. The dominance of the (220) diffraction peak and the absence of other peaks indicate that the TiO_2 nanoarrays are well aligned and have a preferential orientation. Moreover, the prominent (220) plane is beneficial for the photocatalytic process, as the high-index planes are generally considered to have a higher catalytic ability due to the existence of massive active sites.[23,24] The incorporation of MIL-100(Fe) gave rise to new peaks at around 10°, consistent with the crystal structures of pure MIL-100(Fe).[25] The intensities of these peaks are very low, mainly due to the small amount of MIL-100(Fe) in the composite system. The existence of the incorporated MIL-100(Fe) was also confirmed by GIWAXS measurements, where clear differences in the scattering patterns between pristine TiO_2 and the T/M-1.25 composite were observed. As shown in Fig. 2B, for the pristine TiO_2 nanoarrays deposited on an ITO glass substrate, distinct intermittent ring-like scattering patterns with intensity modulations were observed within the q range of >1.79 $Å^{-1}$, originating from the preferential orientation of the TiO_2 nanoarrays on the ITO glass,[26] which is consistent with the SEM and XRD results. In comparison, with the *in situ* growth of MIL-100(Fe), T/M-1.25 exhibits new ring patterns within the q range of 0 to 1.79 $Å^{-1}$ (Fig. 2C), owing to the MIL nanocrystal coating and the porous nature of these crystals. For instance, the rings at q = 0.74 and 0.25 $Å^{-1}$ (Fig. 2D)

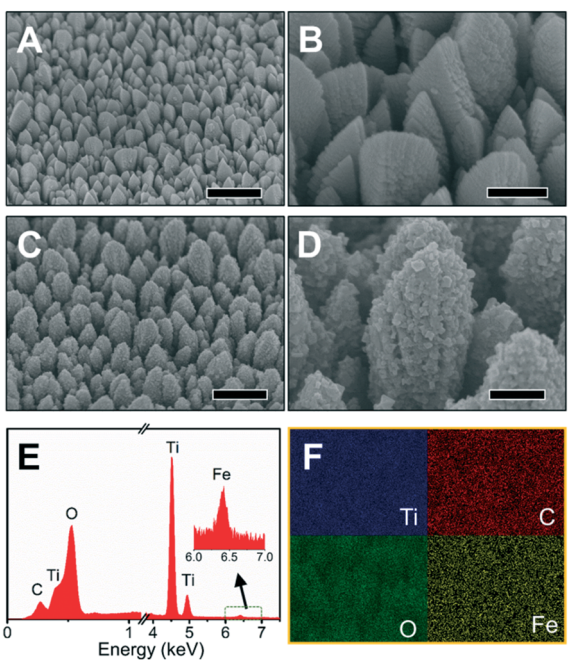

Fig. 1 SEM images of TiO_2 nanoarrays (A and B) and T/M-1.25 (C and D); the EDX spectrum (E) and elemental mapping (F) of T/M-1.25. Scale bars: A and C: 1 μm; B and D: 250 nm.

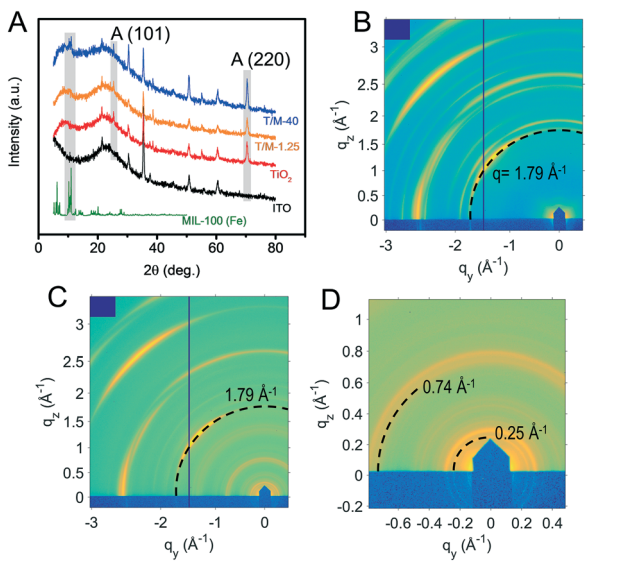

Fig. 2 (A) XRD patterns of the as-prepared samples (A: anatase); GIWAXS profiles of TiO_2 nanoarrays (B) and the T/M-1.25 composite (C and D) on ITO glass.

correspond to the representative pore window size (8.5 Å) and cage size (25 Å) of MIL-100(Fe), respectively.[25]

The UV-vis spectra obtained from the as-prepared samples are shown in Fig. 3A. As shown in Fig. 3A, the pristine TiO_2 nanoarrays only absorb UV light (<400 nm). For the T/M-1.25 composite, the presence of a small amount of MIL-100(Fe) slightly enhances light absorption. With a further increase in the amount of MIL-100(Fe) in the composite, the T/M composites exhibit light absorption over a wide wavelength range (<600 nm). The enhancement in visible-light absorption by MIL-100(Fe) is attributed to the 3d–3d transitions of octahedral $Fe^{III}O_6$.[27] Fig. 3B shows the FT-IR spectra collected from the as-prepared pristine TiO_2 nanoarrays and T/M composites. For the pristine TiO_2 nanoarrays, no discernible IR peaks were observed from 1000 cm^{-1} to 2000 cm^{-1}. Meanwhile, the IR spectra of T/M-1.25 and T/M-20 show strong peaks at 1379, 1450, 1562 and 1621 cm^{-1}, arising from the vibrations of the carboxylate groups.[28]

The amount of MIL-100(Fe) on TiO_2 nanoarrays can significantly affect the surface chemical composition. With a small amount of MIL-100(Fe), the surface of the composite is dominated by the combination of TiO_2 and MIL-100(Fe). Meanwhile, with a high loading of MIL-100(Fe), the surface of the composite is dominated by pure MIL-100(Fe) (*e.g.*, T/M-20, Fig. S2†). The aforementioned difference in the surface configuration could affect the photocatalytic efficiency by changing the light absorption, charge carrier generation and transfer. In this sense, X-ray photoelectron spectroscopy was used to further characterize the surface chemical composition of two representative T/M composites (*i.e.*, T/M-1.25 and T/M-20). The survey spectra of T/M-1.25 and T/M-20 are displayed in Fig. 4A. Owing to the various degrees of coverage of MIL-100(Fe), T/M-1.25 and T/M-20 exhibit different surface chemical compositions. Specifically, two prominent peaks at ~285 eV and ~532 eV were observed for both composites, corresponding to C 1s and O 1s, respectively. T/M-1.25 shows an additional characteristic binding energy of indium (In) element, originating from the ITO glass substrate. With an increased amount of MIL-100(Fe), element Fe was observed on the surface of T/M-20. Fig. 4B displays the high-resolution XPS spectra of C 1 s. For T/M-1.25, there are two main peaks at 284.8 eV and 289.1 eV. In the case of T/M-20, the peak at 289.1 eV disappears, while two additional peaks appear at 283.15 eV and 287.15 eV. The variation in the C 1s spectra between T/M-1.25 and T/M-20 resulted from different MIL-100(Fe) coverages. In particular, in the case of T/M-20 where the TiO_2 nanoarrays are fully covered by MIL-100(Fe) crystals (Fig. S2†), the C 1s spectrum purely originated from MIL-100(Fe). Meanwhile, the variation in C 1s for T/M-1.25 results from the chemical interaction between MIL-100(Fe) and the TiO_2 nanoarrays. The Ti peak in the spectrum of T/M-1.25 was observed at 485.7 eV (Fig. 4C), while no obvious distinct Ti peaks were observed for T/M-20, since the entire surface of the TiO_2 nanoarrays was covered by a thick MIL-100(Fe) layer (Fig. S2†), limiting the transmission of X-rays. For Fe, two dominant peaks were observed for both T/M-1.25 and T/M-20 at 724.65 and 710.65 eV (Fig. 4D), which are attributed to Fe 2p1/2 and Fe 2p3/2, respectively. The difference in band energies between Fe 2p1/2 and Fe 2p3/2 is 14 eV, which is characteristic of Fe_2O_3.[29,30] Due to the increased amount of MIL-100(Fe), more information about Fe was obtained for T/M-20 with an additional shoulder peak appearing at 715.55 eV, corresponding to Fe^{III} in MIL-100(Fe).[30]

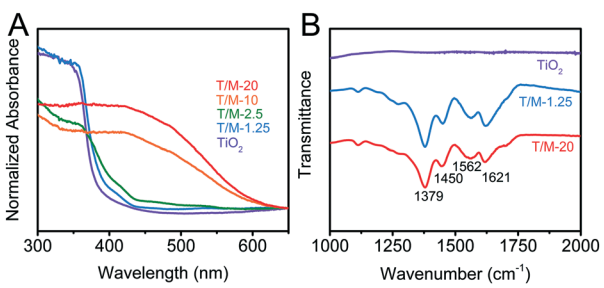

Fig. 3 UV-vis spectra (A) and FT-IR spectra (B) of the samples.

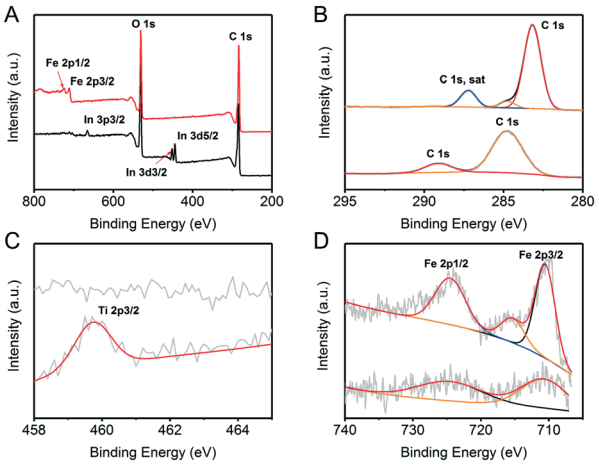

Fig. 4 XPS spectra of T/M-1.25 (lower) and T/M-20 (upper): (A) survey scan; high-resolution spectra of (B) C 1s, (C) Ti 2p and (D) Fe 2p.

The difference in the surface composition resulting from various amounts of MIL-100(Fe) plays a significant role in the photocatalytic ability of the composite, as demonstrated in the following section.

Photodegradation performance

After the detailed characterization, the MIL-100(Fe)/TiO_2 composites were applied for the photodegradation of antibiotics. Tetracycline, one of the most extensively used antibiotics, was chosen as the representative antibiotic.[20] As shown in Fig. 5A, tetracycline was efficiently photodegraded by the T/M composite (T/M-1.25), as evidenced by the decreased intensity of its characteristic peak (357 nm) in the UV-vis spectra. A comparison of the photocatalytic abilities of various catalysts was made (Fig. 5B). As exhibited in Fig. 5B, no significant decrease in tetracycline concentration was observed after 30 min in the dark over all the catalysts, indicating the

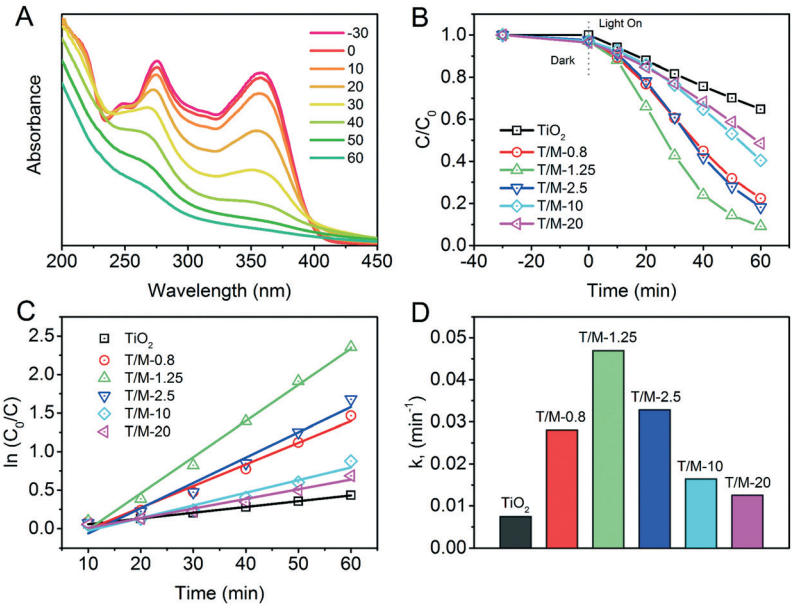

Fig. 5 (A) UV-vis spectra of tetracycline taken during the photocatalytic process in the presence of T/M-1.25 (unit of time: min); (B) photodegradation of tetracycline; (C) kinetics curves of the photodegradation of tetracycline; (D) comparison of reaction rate constants.

negligible adsorption of tetracycline even in the presence of MIL-100(Fe). After 60 min of irradiation, the degradation efficiency of tetracycline for the TiO_2 nanoarrays was about 35.22%. The incorporation of MIL-100(Fe) promotes the photo-degradation of tetracycline. And the highest efficiency was achieved in the case of T/M-1.25 with a removal efficiency of 90.79%, which is about 2.5 times higher than that of the pristine TiO_2 nanoarrays. The kinetics curves shown in Fig. 5C exhibit a linear relationship between $\ln(C_0/C)$ and time, indicating that the photo-degradation of tetracycline follows a pseudo-first-order kinetic model, which could be described as $\ln(C_0/C) = kt$, where k is the reaction rate constant (min^{-1}). The reaction rate constants for various catalysts were determined from Fig. 5C by linear fitting and then summarized in Fig. 5D. Specifically, the reaction rate constants for TiO_2, T/M-0.8, T/M-1.25, T/M-2.5, T/M-10 and T/M-20 are calculated to be 0.00749, 0.02808, 0.04696, 0.03283, 0.01645 and 0.01255 min^{-1}, respectively. All T/M composites exhibit higher efficiencies in the photodegradation of antibiotics than pure TiO_2, which can be attributed to the rapid charge transfer at the interface of TiO_2 and MIL-100(Fe), as verified by photoluminescence and photocurrent transient response measurements in a prior study.[31] Notably, the amount of incorporated MIL-100(Fe) plays a significant role in the photocatalytic efficiency of the T/M composite. Initially, the increased amount of MIL-100(Fe) helps to enhance interfacial charge transfer. However, if the amount of MIL-100(Fe) exceeds the optimal value, the extra MIL-100(Fe) reduces the light absorption of TiO_2 and thus diminishes the excited charge carriers and interfacial charge transfer, leading to a decreased photodegradation efficiency.

During the photocatalytic process, several reactive species could be generated, including electrons (e^-), holes (h^+), superoxide ions ($O_2^{\bullet-}$) and hydroxyl radicals ($^{\bullet}OH$). These species may participate in the photodegradation of tetracycline if thermodynamically favorable. In order to identify the dominant oxidative species, the photocatalytic degradation efficiency was evaluated with the addition of radical scavengers in the solution. In particular, isopropyl alcohol (IPA, 0.2 ml), ethylenediaminetetraacetic acid (EDTA, 10 mM L^{-1}) and *p*-benzoquinone (BQ, 33.3 μmol L^{-1}) were chosen as the scavengers of $^{\bullet}OH$, h^+ and $O_2^{\bullet-}$, respectively.[32] As shown in Fig. 6, the photocatalytic ability of T/M-1.25 was inhibited by 12.0%, 23.1% and 37.5% with the presence of BQ, IPA and EDTA, respectively, indicating the presence of the reactive species (*i.e.*, $O_2^{\bullet-}$, $^{\bullet}OH$ and h^+). Among these species, h^+ appeared to be dominant in the photodegradation of tetracycline, as the addition of the hole scavengers (*i.e.*, EDTA) resulted in the most significant decrease in photocatalytic efficiency.

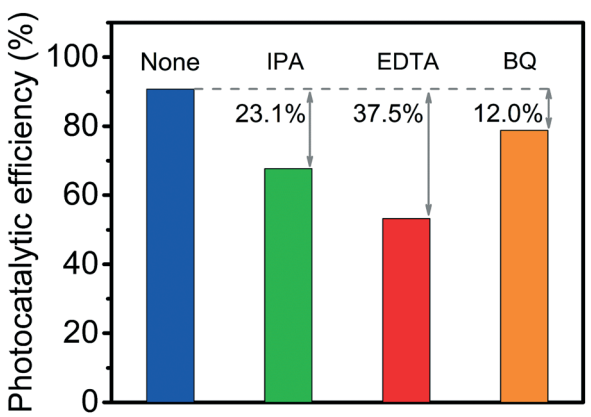

Fig. 6 Photocatalytic degradation of tetracycline over T/M-1.25 with the addition of radical scavengers.

In addition, the MIL-100(Fe)/TiO_2 nanoarrays demonstrated excellent reusability. To be specific, the reusability of the T/M-1.25 composite was evaluated by five cycles of tetracycline photodegradation. After each cycle, the composite film was taken out from the reaction cell with tweezers and washed with DI water to remove the residual reactants, and then dried with an air flow for the next cycle. As shown in Fig. 7, the degradation percentage slightly decreased after the first cycle and then gradually stabilized at ~73% even after 5 cycles, which is still 37.48% higher than that of the pristine TiO_2 nanoarrays.

Taken together, plausible reaction pathways are proposed in Scheme 2 and described as follows. Upon irradiation, TiO_2 is activated with electrons excited from the valence band to the conduction band. On the other hand, MIL-100(Fe) is activated through ligand-to-metal charge transfer and direct excitation of Fe–O clusters.[33] It is well acknowledged that the charge transfer occurs at the interface between MIL-100(Fe) and TiO_2, due to the differences in redox potentials.[31] As a result, the electron/hole recombination was significantly suppressed, leading to abundant free electrons and holes. The porous structure of MIL-100(Fe) enables the accessibility of these electrons and holes, which subsequently react with O_2 and H_2O to form $O_2^{\bullet-}$ and $^{\bullet}OH$, respectively (Scheme 2). The addition of H_2O_2 further facilitates the photocatalytic process by providing more $^{\bullet}OH$ through the reactions with not only the photo-excited electrons but also the Fe^{III} in MIL-100(Fe) to produce Fenton-like reactions (Scheme 2).[34] Finally, all these reactive species, including $^{\bullet}OH$, h^+ and $O_2^{\bullet-}$, synergistically degrade the antibiotics. And the main reactive species responsible for the photodegradation of tetracycline has been identified to be h^+ by the radical trapping experiments.

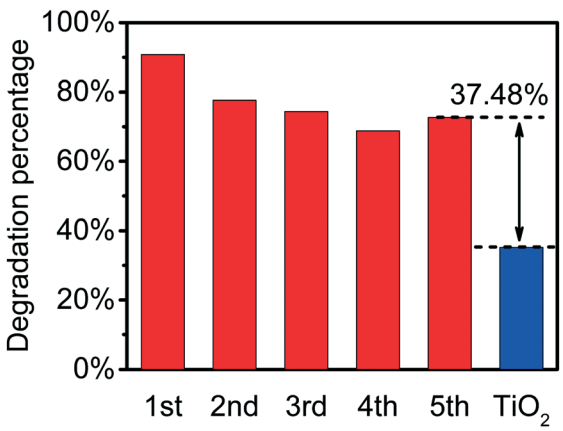

Fig. 7 Recycling photocatalytic tests of T/M-1.25 for the degradation of tetracycline.

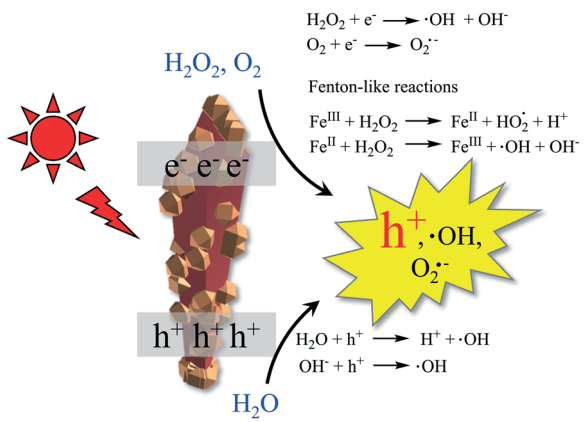

Scheme 2 Proposed reaction pathways.

Conclusions

In summary, highly-oriented 1D MIL-100(Fe)/TiO_2 composite nanoarrays have been synthesized for the photodegradation of tetracycline, where the incorporated MIL-100(Fe) not only enhances the light absorption but also facilitates the electron/hole separation, leading to the promoted photodegradation of tetracycline. Several oxidative species, including $O_2^{\bullet-}$, $^{\bullet}OH$ and h^+, are mainly responsible for the photocatalytic process. Notably, an excessive amount of incorporated MIL-100(Fe) limits the light absorption of TiO_2, which is detrimental to the overall photocatalytic performance. This work demonstrates the use of a 1D TiO_2/MIL composite for the enhanced photodegradation of tetracycline, which will shed new light on photocatalysis by MOF-based composites.

Conflicts of interest

There are no conflicts to declare.

Acknowledgements

The financial supports from the National Science Foundation (CMMI-1727553) and donors of the American Chemical Society (ACS) Petroleum Research Fund (57072-DNI10) are gratefully acknowledged. This research used resources of the Advanced Photon Source, a U.S. Department of Energy (DOE) Office of Science User Facility operated for the DOE Office of Science by Argonne National Laboratory under Contract No. DE-AC02-06CH11357.

Notes and references

1 M. Liu, Y. Zhang, M. Yang, Z. Tian, L. Ren and S. Zhang, *Environ. Sci. Technol.*, 2012, **46**, 7551–7557.
2 K. Kümmerer, *Chemosphere*, 2009, **75**, 417–434.
3 I. Michael, L. Rizzo, C. S. McArdell, C. M. Manaia, C. Merlin, T. Schwartz, C. Dagot and D. Fatta-Kassinos, *Water Res.*, 2013, **47**, 957–995.
4 T. Paul, P. L. Miller and T. J. Strathmann, *Environ. Sci. Technol.*, 2007, **41**, 4720–4727.
5 F. Chen, Q. Yang, Y. Wang, J. Zhao, D. Wang, X. Li, Z. Guo, H. Wang, Y. Deng, C. Niu and G. Zeng, *Appl. Catal., B*, 2017, **205**, 133–147.

6 J. Low, J. Yu, M. Jaroniec, S. Wageh and A. A. Al-Ghamdi, *Adv. Mater.*, 2017, **29**, 1601694.
7 X. Hu, X. Liu, J. Tian, Y. Li and H. Cui, *Catal. Sci. Technol.*, 2017, **7**, 4193–4205.
8 S. Leong, D. Li, K. Hapgood, X. Zhang and H. Wang, *Appl. Catal., B*, 2016, **198**, 224–233.
9 J. Ding, Z. Dai, F. Qin, H. Zhao, S. Zhao and R. Chen, *Appl. Catal., B*, 2017, **205**, 281–291.
10 F. Chen, Q. Yang, X. Li, G. Zeng, D. Wang, C. Niu, J. Zhao, H. An, T. Xie and Y. Deng, *Appl. Catal., B*, 2017, **200**, 330–342.
11 D. Wang and Z. Li, *Res. Chem. Intermed.*, 2017, **43**, 5169–5186.
12 S. Panneri, M. Thomas, P. Ganguly, B. N. Nair, A. P. Mohamed, K. G. K. Warrier and U. S. Hareesh, *Catal. Sci. Technol.*, 2017, **7**, 2118–2128.
13 H. Wang, X. Yuan, Y. Wu, G. Zeng, H. Dong, X. Chen, L. Leng, Z. Wu and L. Peng, *Appl. Catal., B*, 2016, **186**, 19–29.
14 X. He and W.-N. Wang, *J. Mater. Chem. A*, 2018, **6**, 932–940.
15 X. He, C. Yang, D. Wang, S. E. Gilliland Iii, D.-R. Chen and W.-N. Wang, *CrystEngComm*, 2017, **19**, 2445–2450.
16 X. He, Z. Gan, S. Fisenko, D. Wang, H. M. El-Kaderi and W.-N. Wang, *ACS Appl. Mater. Interfaces*, 2017, **9**, 9688–9698.
17 W. J. An, D. D. Jiang, J. R. Matthews, N. F. Borrelli and P. Biswas, *J. Mater. Chem.*, 2011, **21**, 7913–7921.
18 W. J. An, E. Thimsen and P. Biswas, *J. Phys. Chem. Lett.*, 2010, **1**, 249–253.
19 B. Liu and E. S. Aydil, *J. Am. Chem. Soc.*, 2009, **131**, 3985–3990.
20 X.-D. Zhu, Y.-J. Wang, R.-J. Sun and D.-M. Zhou, *Chemosphere*, 2013, **92**, 925–932.
21 W.-N. Wang, W.-J. An, B. Ramalingam, S. Mukherjee, D. M. Niedzwiedzki, S. Gangopadhyay and P. Biswas, *J. Am. Chem. Soc.*, 2012, **134**, 11276–11281.
22 Z. Jiang, *J. Appl. Crystallogr.*, 2015, **48**, 917–926.
23 H. B. Jiang, Q. Cuan, C. Z. Wen, J. Xing, D. Wu, X.-Q. Gong, C. Li and H. G. Yang, *Angew. Chem., Int. Ed.*, 2011, **50**, 3764–3768.
24 C. Luan, Q.-X. Zhou, Y. Wang, Y. Xiao, X. Dai, X.-L. Huang and X. Zhang, *Small*, 2017, **13**, 1702617.
25 P. Horcajada, S. Surble, C. Serre, D. Y. Hong, Y. K. Seo, J. S. Chang, J. M. Greneche, I. Margiolaki and G. Ferey, *Chem. Commun.*, 2007, 2820–2822.
26 T. Brezesinski, J. Wang, S. H. Tolbert and B. Dunn, *Nat. Mater.*, 2010, **9**, 146–151.
27 L. Mitchell, P. Williamson, B. Ehrlichová, A. E. Anderson, V. R. Seymour, S. E. Ashbrook, N. Acerbi, L. M. Daniels, R. I. Walton, M. L. Clarke and P. A. Wright, *Chem. – Eur. J.*, 2014, **20**, 17185–17197.
28 C. Petit and T. J. Bandosz, *Adv. Funct. Mater.*, 2011, **21**, 2108–2117.
29 R. Liang, S. Luo, F. Jing, L. Shen, N. Qin and L. Wu, *Appl. Catal., B*, 2015, **176**, 240–248.
30 H. Zhao, L. Qian, H. Lv, Y. Wang and G. Zhao, *ChemCatChem*, 2015, **7**, 4148–4155.
31 X. Liu, R. Dang, W. Dong, X. Huang, J. Tang, H. Gao and G. Wang, *Appl. Catal., B*, 2017, **209**, 506–513.
32 Z. Yang, X. Xu, X. Liang, C. Lei, Y. Cui, W. Wu, Y. Yang, Z. Zhang and Z. Lei, *Appl. Catal., B*, 2017, **205**, 42–54.
33 V. K. Sharma and M. Feng, *J. Hazard. Mater.*, 2017, DOI: 10.1016/j.jhazmat.2017.09.043.
34 D. Wang, M. Wang and Z. Li, *ACS Catal.*, 2015, **5**, 6852–6857.

Electronic Supplementary Material (ESI) for Catalysis Science & Technology.

Highly-Oriented One-Dimensional MOF-Semiconductor Nanoarrays for Efficient Photodegradation of Antibiotics

Xiang He, [a] Vu Nguyen, [a] Zhang Jiang, [b] Dawei Wang, [a] Zan Zhu, [a] and Wei-Ning Wang*,[a]

[a] Department of Mechanical and Nuclear Engineering, Virginia Commonwealth University, Richmond, Virginia 23219, United States

[b] Advanced Photon Source, Argonne National Laboratory, Argonne, Illinois 60439, United States

*Corresponding Author
Wei-Ning Wang: Tel: 1-(804) 827-4306; Fax: 1-(804) 827-7030; Email: wnwang@vcu.edu

S1. Detailed Information of the TiO_2 Nanoarrays

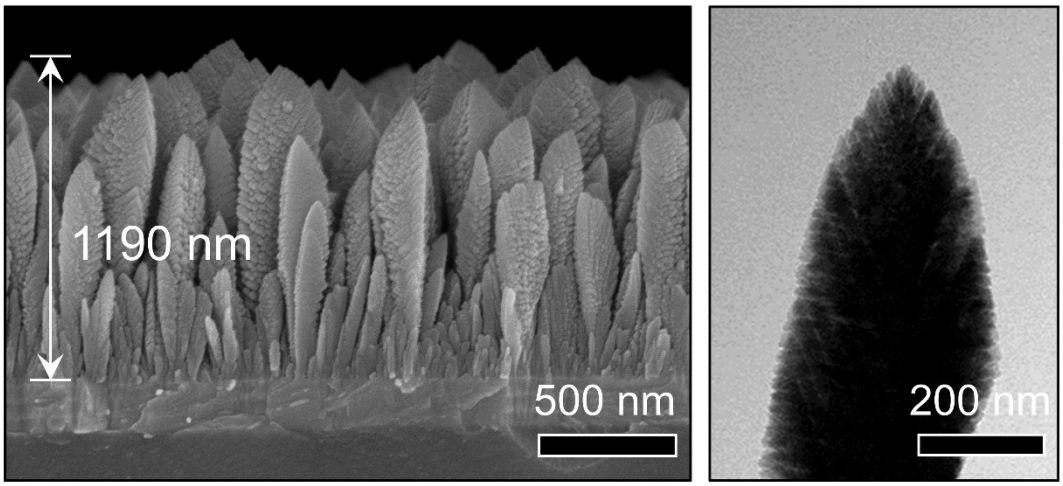

Figure S1. Left: SEM image of the cross section of the pristine TiO_2 nanoarrays; Right: TEM image of the pristine TiO_2.

S2. SEM Images of T/M-20 Composite

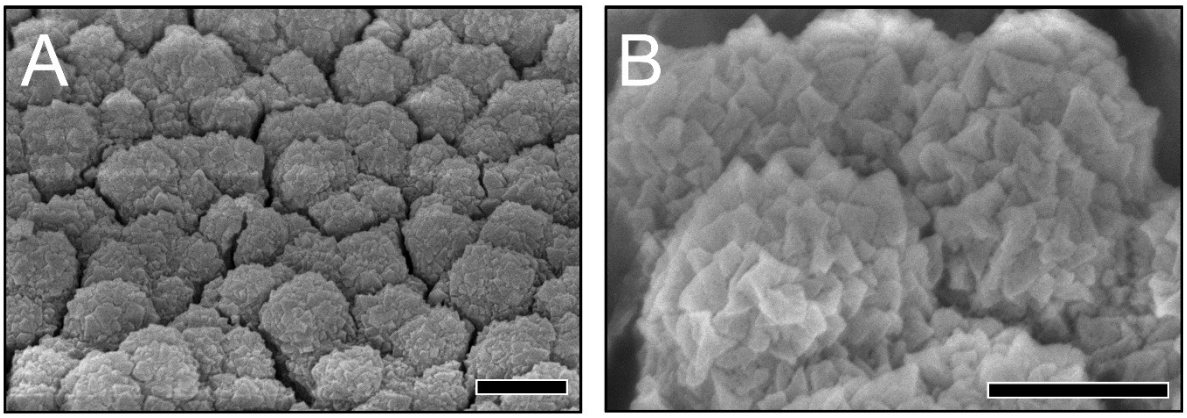

Figure S2. SEM images of T/M-20 composite. A: low-magnification, B: high-magnification. Scale bars: A: 1 μm, B: 500 nm.